MODELING LIFT-OFF DEPOSITION

by

LeRoy Winemberg

Memorandum No. UCB/ERL M84/112

15 December 1984

MODELING LIFT-OFF DEPOSITION

by

LeRoy Winemberg

Memorandum No. UCB/ERL M84/112

15 December 1984

ELECTRONICS RESEARCH LABORATORY

College of Engineering
University of Califonria, Berkeley
94720

Modeling Lift-Off Deposition

LeRoy Winemberg

Dept. of Electrical Engineering and Computer Sciences
and the Electronics Research Laboratory,
University of California, Berkeley, CA 94720

ABSTRACT

The effects of tooling and resist parameters on the lift-off metallization process are investigated and modeled through computer simulation with extensions to the SAMPLE program. Also, simple equations are proposed for predicting resist and tooling effects on the final metal profile. The formation of metal "feet" resulting from the deposition of metal on the resist sidewalls is used to judge the quality of the lift-off process. Using the height of the metal foot as a figure of merit, simulation studies and the proposed equations are used to establish design guidelines for lift-off metallization. Through the use of these guidelines, the proper balance between the tooling configuration and the resist profile necessary for a successful lift-off process can be found.

December 12, 1983

Modeling Lift-Off Deposition

LeRoy Winemberg

Dept. of Electrical Engineering and Computer Sciences
and the Electronics Research Laboratory,
University of California, Berkeley, CA 94720

1. Introduction

As IC process technology pushes toward smaller device geometries and higher packing densities, multilevel metallization of these circuits is becoming an increasingly difficult task. Blanket metallization of the wafer with subsequent photomasking and etching steps is the most common method of defining metal lines. But to achieve 1-2 micron metal linewidths, the above method must overcome two serious obstacles. First is the photolithographic problem of imaging on a highly reflective metals. Second, anisotropic etching of the metal or metal alloy is necessary to attain 1-2 micron lines. These obstacles can be avoided through the use of the metal lift-off technique. The lift-off metallization process involves the deposition of metal over a photoresist stencil, followed by the removal or "lifting-off" of the undesired metal by dissolving the photoresist.

A simple single-step lift-off process was proposed in 1980 by Hatzakis et al [1]. Since then, both the requirements and the limitations of the metal lift-off process have

been studied through experimentation for planetary evaporation [2], [3] and for sputtering [4]. Simulation tools are available for systematically studying depositions but they have not been well utilized for characterizing the lift-off process. The IC process simulation program SAMPLE [5] is convenient for both analyzing the trade-offs between key factors in lift-off and characterizing established lift-off processes.

This paper analyzes, through computer simulation and geometric analysis, the effects of both resist and tooling parameters on the lift-off metallization pattern profile. A comparison of simulated and experimental lift-off profiles is performed to establish the accuracy of the simulation program. A series of equations derived from geometric analysis of the resist and tooling configurations are proposed for modeling the lift-off process. These equations and simulation results are then used to create a series of design guides. These design guides help establish the proper balance between the tooling configuration and the resist profile necessary to obtain a useful lift-off metallization process.

2. Key Factors in Lift-Off

2.1. Step Coverage

The ideal deposition conditions for lift-off are: 1) normal incidence of the incoming metal flux, 2) low temperature (to prevent resist degradation), and 3) low pressure. While the second condition is unavoidable for the above mentioned reason, variations in the other two conditions are necessary if acceptable step coverage is to be achieved. A main criterion for step coverage is the cross-sectional thickness of the metal along the face of the step. This thickness is defined in Figure 1 as tstep, and is important since it determines the current density in the aluminum line at the step. For nearly normal incidence of the aluminum flux, tstep is related to the total aluminum thickness deposited, tm, by

$$t_{step} = t_m \cos\theta \qquad (1)$$

where θ is the step angle. Thus the total metal thickness required, for a given step angle, to prevent high current density-related problems such as electromigration from occurring at the step can be calculated from Equation (1).

As the distribution of incoming metal flux becomes distributed around the normal to the wafer, more metal will be deposited on the step face and Equation (1) will become invalid. Hence for a process that requires a fixed metal

thickness and yields steps with large step angles that cannot be varied, the distribution of incident metal flux must be varied to attain a desired value of tstep. But this means moving away from the "ideal" lift-off condition of normal incidence. It is under these circumstances that a balance must be found between lift-off and step coverage. Fortunately this limiting case is usually not encountered since either the metal thickness or step angle can be adjusted.

2.2. System Design - Throughput

If high throughput is desired, variations from normal incidence must be tolerated. These variations from normal incidence can be minimized through the use of an evaporator with an electron beam or rf-heated source and a rotating dome. Such an evaporator is depicted in Figure 2. By finding the proper combination of wafer position (α^*_w), distance from the centerline to the source (d), dome height (r), and dome radius (Rd),minor variation from normal incidence can be attained. The smaller the ratio of d to r, the more normal the incidence of the incoming metal flux. The effects on lift-off metallization of varying both the ratio of d to r, and the wafer position α^*_w for Rd>r is studied through SAMPLE simulation and geometric analysis in Section 4.

The variations from normal incidence, although minor, can lead to deposition of metal on a portion of the resist

sidewall as shown in Figure 3. While this metal "foot" will not prevent successful lifting of the unwanted metal, it can pose a problem for a subsequent passivation layer. The lack of metal deposition on the right resist sidewall (Fig. 3) illustrates the asymmetric distribution of the incoming metal flux with respect to the wafer normal. This asymmetric distribution occurs when the metal line runs parallel to the evaporator centerline. Conversely, a symmetric deposition will take place when the metal line points toward the evaporator centerline. A simulated symmetric deposition is illustrated in Figure 4. Here the metal is deposited on both resist sidewalls, but the height of the metal feet is reduced compared to the metal foot in Figure 3.

The deposition of metal on the resist sidewalls can be eliminated by reducing either the ratio of d to r, or α_w. These reductions serve to decrease the angular distribution of the metal flux about the wafer normal. If, however, neither the ratio of d to r nor α_w can be further reduced, then the photoresist profile must be modified in order to eliminate the metal feet.

2.3. Photoresist Profile Requirements

A typical photoresist profile for lift-off is shown in Figure 5. This type of profile is obtained for photoresist prepared as described in [1]. Note that the key parameters for the resist profile are the angles θ_1 and θ_2 as defined in

Figure 5. The angle θ_2 is a measure of the degree of "overhang" the resist profile possesses. The extent of resist "skirt" is indicated by the angle θ_1. Together, angles θ_1 and θ_2 determine the size and the shape of the metal feet. By increasing the overhang angle θ_2 the formation of metal feet can be prevented. If θ_2 is not sufficiently large to preclude the deposition of metal on the resist skirt, then the height h1 (Fig. 5) of the metal foot can be diminished by decreasing θ_1. Thus both θ_1 and θ_2 determine the metal foot height h1. The thickness h2 of the metal at the base of the foot is dependent on the value of θ_2. The dependence of h1 and h2 on the photoresist angles θ_1 and θ_2 is studied through simulation in Section 4.

Relationships between the angles θ_1 and θ_2, and the metal foot parameters h1 and h2 can be derived through geometric considerations. In Figure 5, the angles α_1 and α_2 represent the maximum angular excursions of the source from the wafer normal. Angle α_1 is measured counterclockwise from the normal and angle α_2 is measured clockwise. For an asymmetric deposition $\alpha_1 \neq \alpha_2$, and for the symmetric case $\alpha_1 = \alpha_2$. Let point A represent the origin, and define the x and z directions as in Figure 5. The metal foot height h1 can now be defined as the z-coordinate of the highest point on the resist skirt that is not shadowed by the overhang, point C. Line CD in Figure 5 thus forms an angle α_2 with the wafer normal and is the boundary line for shadowing by the resist overhang. Points on the line AB above and to the left of line CD are

completely shadowed from the source, and points below and to the right of CD can see part of the source. Hence h1 is the z-coordinate of the point of intersection of lines AB and CD.

An equation for h1 can now be derived. Let point C have the coordinates (Xr,Zr) and point D the coordinates (Xd,0) where Xr>0 and Xd<0. With these definitions, Xd is given by

$$-x_d = z_r \tan \alpha_2 - x_r \qquad (2)$$

where the value of Zr is assumed to be known (approximately the resist thickness), and xr is given by

$$x_r = z_r \tan(\theta_2 - 90^\circ) = -z_r \cot(\theta_2). \qquad (3)$$

Note that in all equations, every angle is positive. Using Equations (2) and (3), the equation for line CD can be expressed as

$$z = (\cot \alpha_2)\, x + z_r (1 + \cot \alpha_2 \cot \theta_2). \qquad (4)$$

The equation for line AB is given by

$$z = -(\tan \theta_1)\, x \qquad (5)$$

or

$$x = (-\cot \theta_1)\, z. \qquad (6)$$

Define the point of intersection of lines AB and CD as (x1,h1). Substituting this point into Equations (4) and (6)

and then solving for h1 yields

$$h_{1_{left}} = 3r\left[\frac{\tan\alpha_2 + \cot\theta_2}{\tan\alpha_2 + \cot\theta_1}\right]. \qquad (7)$$

Note that this is the metal foot height at the left resist sidewall. Similarly, the metal foot height at the right resist sidewall is given by

$$h_{1_{right}} = 3r\left[\frac{\tan\alpha_1 + \cot\theta_2}{\tan\alpha_1 + \cot\theta_1}\right]. \qquad (8)$$

For a symmetrically oriented metal line, $\alpha_1 = \alpha_2$ and Equations (7) and (8) become identical.

From Equations (7) and (8), the conditions necessary to eliminate the formation of metal feet become apparent. These conditions are

$$\tan\alpha_1 \leq -\cot\theta_2$$

and

$$\tan\alpha_2 \leq -\cot\theta_2$$

or

$$\alpha_1 \leq \theta_2 - 90^\circ \qquad (9a)$$

and

$$\alpha_2 \leq \theta_2 - 90^\circ. \qquad (9b)$$

If both these conditions are met, no metal will be deposited on the resist skirt. An alternative condition for eliminating the metal feet is

$$\theta_1 = 0^\circ. \qquad (10)$$

This condition occurs when no resist skirt exists.

An equation for the metal thickness at the base of the foot, h2, can be derived following a similar treatment as above. At point M' in Figure 5, the metal just begins to grow at its maximum rate as the entire source has just become unshadowed by point C''. At point D', the entire source becomes shadowed by C'. Thus as one moves from D' to the left, more and more of the source becomes exposed and the metal grows thicker. If no resist skirt is present, this increase in the metal thickness as one moves to the left of D' can be approximated by a straight line from D' to M'. With a resist skirt present, a metal foot forms. When the metal foot first begins to grow, its base is located at A'. As the metal continues to grow, the top of the base represented in Figure 5 as point H' moves toward point C'. Thus point H' can be expressed as approximately the point of intersection of lines AC' and D'M'.

Let us define the coordinates of point A' as (0,0), point C' as (Xc,Zr), point M' as (Xm,Zm), and point D' as (Xd',0) where Xc<0, Xm<0, and Xd'>0. The values of Xd' and Xm are given by

$$x_{d'} = z_r \tan\alpha_1 + x_c \qquad (11)$$

and

$$x_m = x_c - z_r \tan\alpha_2 \qquad (12)$$

where

$$x_c = z_r \cot \theta_2 \qquad (13).$$

and Zr is assumed to be known (approximately the resist thickness). Zm is the metal thickness desired. Again note that all angles are positive. The equation for line D'M' can be expressed as

$$z = \frac{-z_m}{z_r(\tan\alpha_1 + \tan\alpha_2)}\left(x - z_r(\tan\alpha_1 + \cot\theta_2)\right). \qquad (14)$$

The equation for line AC' is given by

$$z = -(\tan\theta_2)\,x \qquad (15)$$

or

$$x = -(\cot\theta_2)\,z. \qquad (16)$$

Define the coordinates of point H' as (x2,h2). Substituting this point into Equations (14) and (16) and then solving for h2 yields

$$h_{2_{right}} = \frac{z_m(\tan\alpha_1 + \cot\theta_2)}{\left[\tan\alpha_1 + \tan\alpha_2 + \left(\frac{z_m}{z_r}\right)\cot\theta_2\right]}. \qquad (17)$$

Similarly, the value of h2 for the left metal foot is given by

$$h_{2_{left}} = \frac{z_m(\tan\alpha_2 + \cot\theta_2)}{\left[\tan\alpha_1 + \tan\alpha_2 + \left(\frac{z_m}{z_r}\right)\cot\theta_2\right]}. \qquad (18)$$

Again, for a symmetrically oriented line, $\alpha_1 = \alpha_2$ and Equations (17) and (18) become identical. When no metal deposition on the resist skirt takes place, h2 becomes a meaningless

parameter.

The effects of tooling and resist parameters on the lift-off process can be clarified by simplifying the equations for h1 and h2 derived above. The source incidence angles α_1 and α_2 can be expressed in terms of the tooling parameters d (source position), r (dome height), α_w (wafer position), and Rd (dome radius). α_1 and α_2 are given by

$$\alpha_1 = \frac{d}{r} - \left(1 - \frac{r}{R_d}\right)\alpha_w \qquad (19a)$$

$$\alpha_2 = \frac{d}{r} + \left(1 - \frac{r}{R_d}\right)\alpha_w . \qquad (19b)$$

With these equations, the effect of tooling configuration on the distribution of the incident metal flux becomes clear. Using mathematical approximations and normalizing to the metal thickness Zm, the left metal foot height h1 is given by

$$\frac{h_{1\,left}}{Z_m} = \left(\frac{Z_r}{Z_m}\right)\frac{1 - \frac{\Delta\theta_2}{\alpha_2}}{1 + \frac{\Delta\theta_1}{\alpha_2}} \qquad (20)$$

where $\theta_1 = 90 - \Delta\theta_1$, $\theta_2 = 90 + \Delta\theta_2$, and α_2 is given above. Similarly, the thickness of the metal at the base of the metal foot h2 is given by

$$\frac{h_{2\,left}}{Z_m} = \frac{\left(1 - \frac{\Delta\theta_2}{\alpha_2}\right)\left(1 + \left(\frac{Z_m}{Z_r}\right)\frac{1}{(1 + \alpha_1/\alpha_2)}\frac{\Delta\theta_2}{\alpha_2}\right.}{\left(1 + \alpha_1/\alpha_2\right)} . \qquad (21)$$

Define the horizontal distance between points C' (Xc,Zr) and J' (Xj,h1) as Wtop. Wtop is thus a measure of the increase in linewidth over the desired linewidth resulting from the formation of metal feet. Obviously it is desirable to reduce Wtop. Through geometric analysis, Wtop/Zm can

be expressed as

$$\frac{\Delta W_{top}}{Z_m} = \frac{Z_r}{Z_m}\left[\Delta\theta_2 + \frac{\Delta\theta_1\alpha_2}{\Delta\theta_1+\alpha_2}\left(1-\frac{\Delta\theta_2}{\alpha_2}\right)\right] \quad (22)$$

Thus through Equations (19)-(22), the impact of key resist and tooling parameters on the lift-off process becomes transparent. The effect of θ_2 on h1, h2, and Wtop is illustrated in Figure 6. Note that the h1 and h2 curves cross at $\Delta\theta_2/\alpha_2=0.6$, and stay close together from that point onward. At $\Delta\theta_2/\alpha_2=0.6$, h1=Zm/3. The magnitude of Wtop increases only slightly for increasing $\Delta\theta_2/\alpha_2$.

Figure 6 shows the desirability of a large resist undercut. However, for small, closely spaced metal lines, problems with resist adhesion limit the degree of undercut allowed. As the undercut increases, the width of the photoresist pattern at its base decreases. Hence as the lines get more closely spaced, the resist base gets narrower and eventually the resist structure will just fall over. Therefore, while a large resist undercut angle θ_2 is desirable, for small linewidths the conditions of Equation (9) are unfeasible. An alternative set of conditions would be for $\Delta\theta_2>0.6\alpha_1$ and $\Delta\theta_2>0.6\alpha_2$. As mentioned above, h1 and h2 are close in value and steadily decreasing in this range of overhang angles. Also in this range, the metal foot height h1 is maintained below one third of the total metal thickness Zm. Using these conditions, the deleterious effects of the metal feet can be minimized for a given set of process constraints.

2.4. Covering Lifted Metal

Passivation of the lifted metal line is necessary to prevent corrosion of the aluminum line and also to insulate one level of aluminum from another if a multilevel metallization scheme is used. The presence of metal feet on the sides of a metal line poses an obstacle to successful passivation. Figure 7 depicts an aluminum line with a large metal foot on the left, and no metal foot on the right. The line is covered with one micron of sputtered oxide. It can be seen in Figure 7 that the metal foot causes a crack in the insulator which reaches all the way down to the aluminum. This crack is a probable source of either corrosion, an interlevel short, or both.

The severity of the oxide crack is reduced when the metal foot height equals the metal thickness at the base of the metal foot, i.e., h1=h2. This case is illustrated in Figure 8. Large cracks form at the base of the metal line, however they do not reach the aluminum. Even for no metal foot (Fig.7), a crack in the insulator forms due to shadowing effects. The metal feet increase the shadowing at the base of the metal line resulting in larger cracks. Thus it is desirable to eliminate the metal foot, h1=0, or minimize its height.

3. Results of Simulation and Experiment

A comparison of simulation and experimental results was performed to establish the accuracy of the simulation model. The experiments were performed at IBM-Manassas, and were part of a collaborative effort aimed at modeling the lift-off process. The resist profiles were obtained by soaking 2.15 microns of photoresist in chlorobenzene for 18 minutes. After exposure, the photoresist was developed for 105 seconds. The resultant resist structure is shown in Figure 9. The wafers were then placed in an evaporator and 1.0 micron of Al/Cu/Si was deposited. Lines in both the symmetric and asymmetric orientations underwent metallization. The wafers were then cleaved and SEM micrographs taken of the blanket metallization pattern for both orientations. Lift-off was then performed and the cross-sections of the metal lines were again observed with a scanning electron microscope and micrographs taken.

Figure 10 shows three SEM micrographs of a symmetrically oriented metal line before and after lift-off. Note that the deposition of metal on the resist skirt results in the symmetric formation of metal feet on the metal line. Figure 11 depicts four SEM micrographs of an asymmetrically oriented line before and after lift-off. The micrographs of the metal profiles after lift-off were taken looking in from the opposite end of the metal line shown in the blanket metallization micrographs. Thus Figure 11b corresponds to Figure 11a, and Figure 11d corresponds to Figure 11c. Note that the left metal foot (Figs.11c and 11d) is larger than

the right metal foot (Figs. 11a and 11b) as expected for the asymmetric deposition. In the SEM's shown in Figures 10 and 11, what appears to be an outward curve of the metal at the top resist lip is mostly due to the depth of focus of the SEM. The actual edge of the metal has only a slight outward curve.

Simulation of the above lift-off depositions was carried out using the program SAMPLE. The lift-off resist profiles and the tooling configuration were entered into the program, and the depositions simulated. Figure 12 depicts a SAMPLE simulation of a metallized lift-off profile for a symmetrically oriented line. The tapered sides of the metal line, and the size and shape of the metal feet in the simulated profile are in very good agreement with their experimental counterparts in the actual profile (Fig. 10). Simulation of an asymmetric lift-off deposition is shown in Figure 13. The sloped metal edge seen in Figure 11a is simulated very well in Figure 13. Also, the simulated metal feet in Figure 13 are very similar to the actual metal feet shown in Figures 11b and 11c.

Very good agreement between experiment and simulation has been demonstrated. The formation of metal feet predicted by the computer simulation has been verified experimentally. Also, asymmetrical effects due to the tooling configuration have been predicted by SAMPLE and also verified experimentally. Thus the accuracy of the

simulation has been established, and further SAMPLE simulation will be used in Section 4 to study the effects of the tooling and resist parameters discussed in Section 2.

4. Design Studies

Using the simulation program SAMPLE, the effects of various tooling and resist parameters on the formation of metal feet during lift-off metallization can be studied. To be able to carry out this study, code was added to SAMPLE to allow the simulation of metal deposition on symmetrically oriented lines. The deposition model assumes the density of metal flux decreases as the square of the distance from the source. Also, cosine emission from the source is assumed. For the simulations, the deposition of 1 micron of aluminum on a photoresist pattern 2.15 microns thick was performed. A dome height of 26 inches and a dome radius of 28 inches were used. The source distance d was varied. The height of the metal foot h1, and the thickness of the foot at its base h2, are used as figures of merit in evaluating the lift-off process. As discussed in Section 2.3, we would like h1 to be zero or, if h1 is to be nonzero, we would then like for h1 to equal h2. The values of h1 and h2 are measured from simulation results while key resist and tooling parameters are varied. In addition, the values of h1 and h2 are also calculated from Equations (7), (8), (17), and (18) derived in Section 2.3. The measured and calculated values of h1 and h2 are then plotted to clarify the impact of the resist and tooling parameters on the lift-off process.

Figures 14 and 15 illustrate the effect of tooling parameters on h1 and h2. The evaporator configuration

simulated is that depicted in Figure 2. In Figure 14, the ratio of the distance of the source from the center line, d, to the dome height, r, is varied for a fixed wafer position α_w=15, and a fixed resist profile. Note that as the value of d/r increases, the angular distribution of the incident metal flux also increases resulting in more metal deposition on the resist skirt and thus larger values of h1. Hence to reduce h1, the ratio of d to r must also be reduced. Note in Figure 14 the good agreement between the simulation and theoretical (geometric) data points. The worst agreement between these points is in Figure 15 for large values of α_w. Good agreement between theory and simulation exists for all other design cases. The simulation data points will thus be omitted from the other design graphs to make them easier to read.

Figure 15 illustrates the effect of the wafer position on the values of h1 and h2 for all other tooling and resist variables fixed. It is apparent in Figure 15 that the condition of h1=0 cannot be met. Still, the value of h1 can be reduced by decreasing the value of α_w.

The effect of the ratio of source position to dome height (d/r) on h1-left and h2-left with the resist overhang angle θ_2 as a parameter is illustrated in Figure 16. As expected, the value of h1 and thus the amount of deposition on the resist skirt decreases as the resist overhang (θ_2) increases. It is also interesting to note in Figure 16 how

the dependence of h2-left on d/r changes as the resist overhang (θ_2) changes.

Finally, the effect of the ratio d/r on h1-left and h2-left with the skirt angle θ_1 as a parameter is shown in Figure 17. As the skirt angle is increased, more of the resist sidewall is exposed to the source leading to increased deposition on the skirt and a larger value of h1-left. It can be observed in Figure 17 that variations in the skirt angle have little effect on h1-left for $d/r<0.2$. But for values of $d/r>0.2$, the impact of the skirt angle on the magnitude of h1-left increases. Hence the value of θ_1 should be minimized in order to decrease as much as possible the magnitude of h1-left. Note that the value of θ_1 has very little (simulation results) or no (Equation (18)) effect on the magnitude of h2-left.

The information displayed in Figures 14-17 characterizes the lift-off process. In using the metal foot parameters h1 and h2 as measures of the quality of a lift-off process, Figures 14-17 can be used either to optimize an established lift-off metallization process or act as guidelines in instituting a new lift-off process. Thus through the use of the simulation tool SAMPLE, a lift-off metallization process can be modeled, and design guides established for finding the proper balance between critical photoresist and tooling parameters.

5. Summary

The important factors in lift-off metallization technology have been reviewed, and their overall impact on the lift-off process discussed. With this information, the need for proper characterization and modeling of the lift-off process was established.

The IC process simulation program SAMPLE was proposed as a means of obtaining the data necessary to model lift-off depositions. Comparisons of experimental and simulation profiles were performed and the accuracy of the simulation program confirmed. Simulations were then carried out to model the effects of various tooling and resist parameters. Further, some simple equations were derived through geometric analysis and also used to model the effects of the resist and tooling. These transcendental equations were compared to simulation results and good agreement was achieved. The transcendental equations were also simplified in order to clarify the effects of tooling and resist parameters on lift-off metallization.

These models provide guidelines for establishing or improving a lift-off process. The guidelines are: 1) the resist skirt angle θ_1 does not have a significant effect on the lift-off process when the resist overhang angle θ_2 is large. Otherwise, it is desirable to minimize the effect of the resist skirt by reducing θ_1. 2) Keep the ratio of source position to dome height, d/r as small as possible to

maintain nearly normal incidence of the incoming metal flux. 3) For an evaporator with dome radius larger than dome height, best lift-off results are obtained when the wafer position α_w is small. Thus placing wafers on the inner or middle tier of the dome is advisable. 4) For fixed tooling and resist parameters, symmetrically oriented lines yield better metal profiles than do asymmetric lines. And finally, 5) the resist overhang angle θ_2 should ideally be greater than or equal to the maximum angular excursion of the source from the wafer normal, α_1^* or α_2^*. For narrow metal lines closely spaced, the amount of resist overhang is restricted by resist adhesion considerations. Taking this restriction into account, a comprimise on the requirement for the resist overhang angle is given by

$$(\theta_2 - 90^\circ) \geq 0.6\,\alpha_1 \quad \text{for } \alpha_1 > \alpha_2$$

$$(\theta_2 - 90^\circ) \geq 0.6\,\alpha_2 \quad \text{for } \alpha_1 < \alpha_2 .$$

In this range of θ_2, the maximum foot height is one third of the total metal thickness deposited. Thus with the use of these guidelines, a successful lift-off metallization process can designed and implemented.

6. Appendix

A planetary evaporation system is shown in Figure 18. Since rotation around the center line does not effect the deposition [6], it can be assumed that the planet only rotates about its own axis. For ease of calculation, the planet is held fixed and the source is rotated around the planet's axis as illustrated in Figure 18. Also note in Figure 19 the definition and orientation of the "A" step. The A steps are symmetric and the metal coverage of each is identical. The metal growth equations for the symmetric orientation are listed at the very back of this report. The documentation for this code will be given in G. Addiego's M.S. report.

To simulate a symmetric planetary deposition using SAMPLE, Trial 50 with mtype=5 and mrsl=2 must be specified. It is important to note that the value of rsl must be given when a symmetric deposition is to be simulated. An example of an input file to SAMPLE for a symmetric deposition is shown in Figure 20. The resultant simulated profile is shown in Figure 21. This same deposition was published in [6]. The agreement is excellent between the SAMPLE simulation and the profiles published in [6] (see Fig. 8 in [6]).

7. Acknowledgements

I would like to thank my fellow students in the SAMPLE group for their frequent advice, their support, and their friendship. Thanks also go to J. Barber, M. Nanda, and J. Kristoff of IBM-Manassas for providing the SEM's used in this report. Special thanks go to my research advisor, Andy Neureuther. His patience, interest, and guidance made this report possible.

8. References

[1] M. Hatzakis, B.J. Canavello, and J.M. Shaw, "Single Step Optical Lift-Off Process," IBM J. Res. Develop., vol. 24, no. 4, July 1980.

[2] T. Batchelder,"Simple Metal Lift-Off Process for 1 Micron Al/5%Cu Lines," Solid State Technology, vol. 25, no. 2, Feb. 1982.

[3] Y. Homma, A. Yajima, and S. Harada,"Feature Size Limit of Lift-Off Metallization Technology," 1981 IEDM Tech. Dig., Dec. 1981.

[4] T. Serikawa and T. Sakurai,"The Size Effect of Lift-Off Metallization of Sputtured Aluminum Films," IEEE Trans. Electron Devices, vol. ED-29, no. 5, May 1982.

[5] W.G. Oldham, A.R. Neureuther, C. Sung, J.L. Reynolds, and S.N. Nandgaonkar,"A General Simulator for VLSI Lithography and Etching Processes: Part II - Application to Deposition and Etching," IEEE Trans. Electron Devices, vol. ED-27, no. 8, Aug. 1980.

[6] I.A. Blech, D.B. Fraser, and S.E. Hasyko,"Optimization of Al Step Coverage through Computer Simulation and Scanning Electron Microscopy," J. Vac. Sci. Technol., vol. 15, no.1, Jan/Feb. 1978.

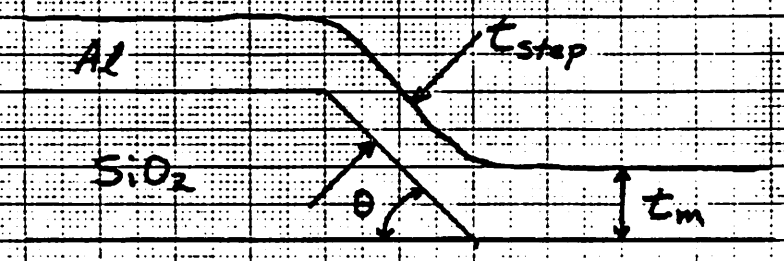

Figure 1 - Definition of step-coverage parameters.

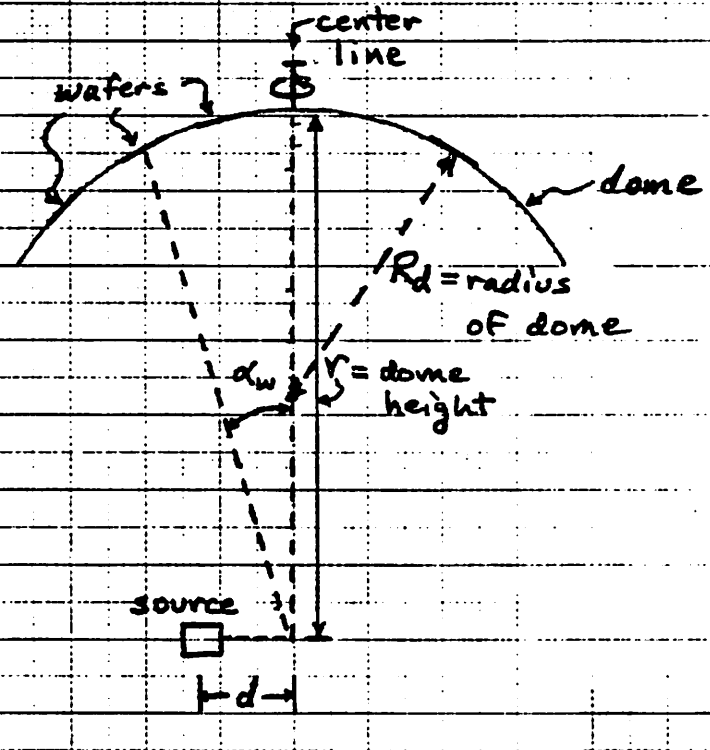

Figure 2 - Evaporator with rotating dome and off-axis source.

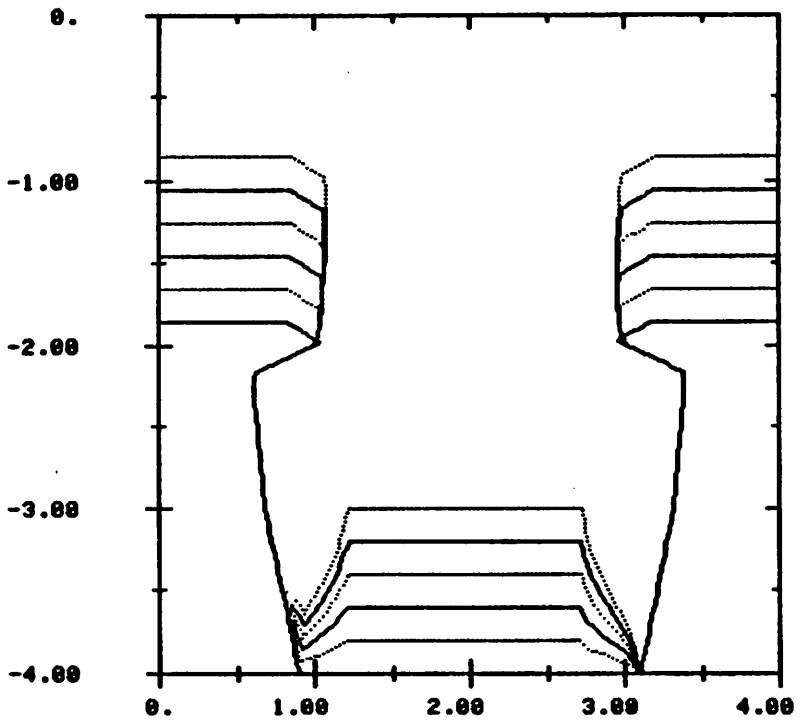

Figure 3 - SAMPLE simulation of an asymmetric lift-off deposition.

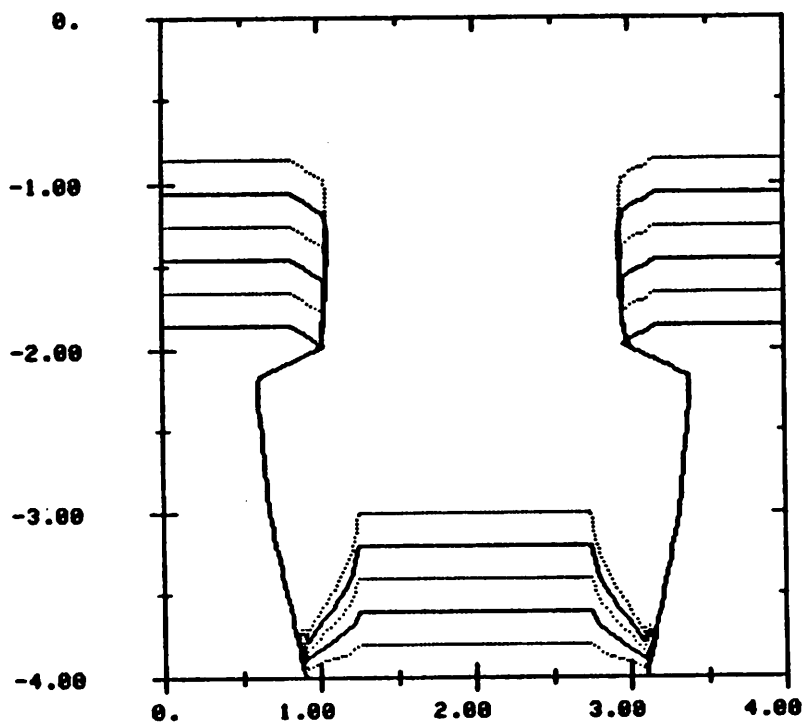

Figure 4 - SAMPLE simulation of a symmetric lift-off deposition.

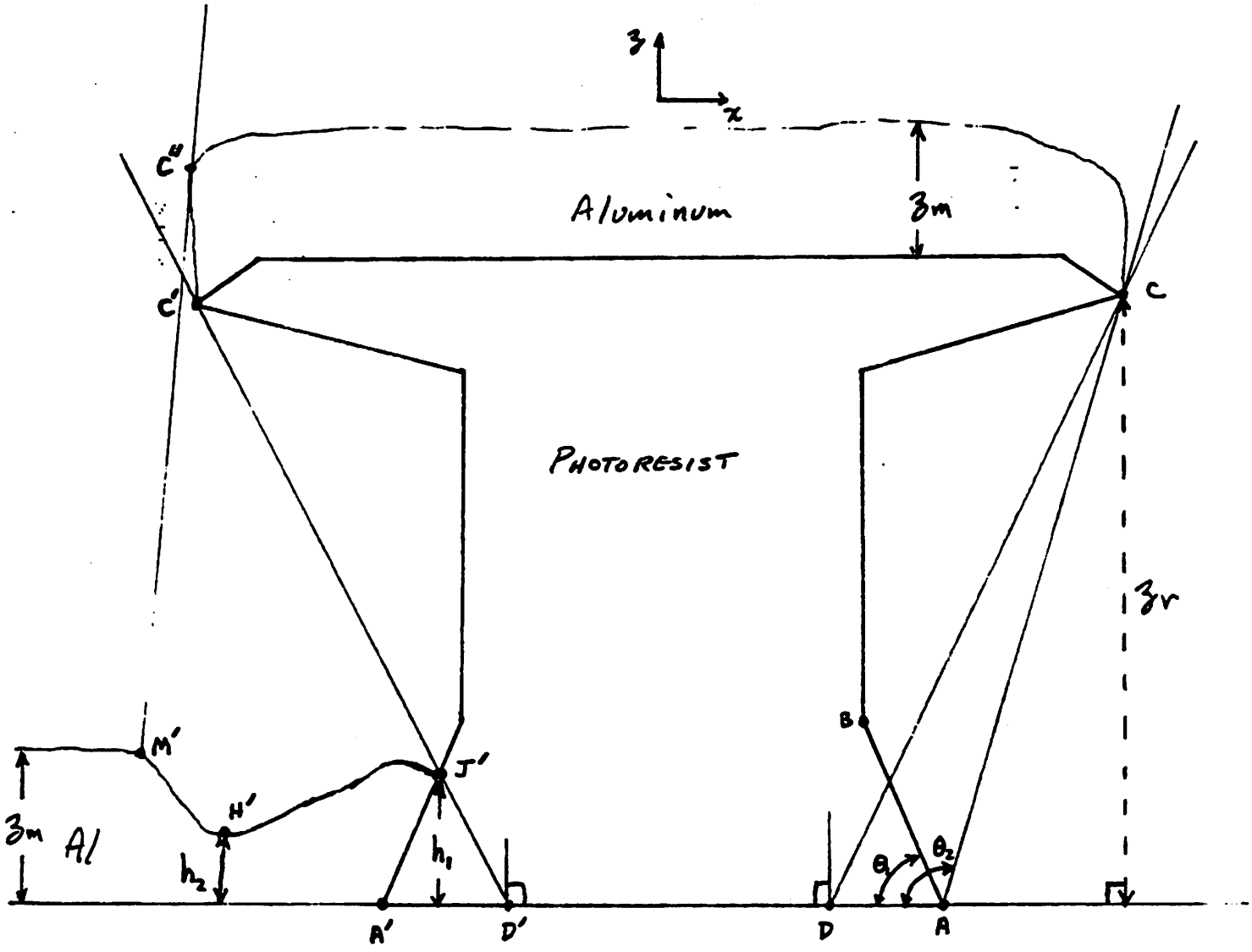

Figure 5 - Typical chlorobenzene-treated photoresist profile. Note that the resist thickness is ~ zr, and the metal thickness is zm.

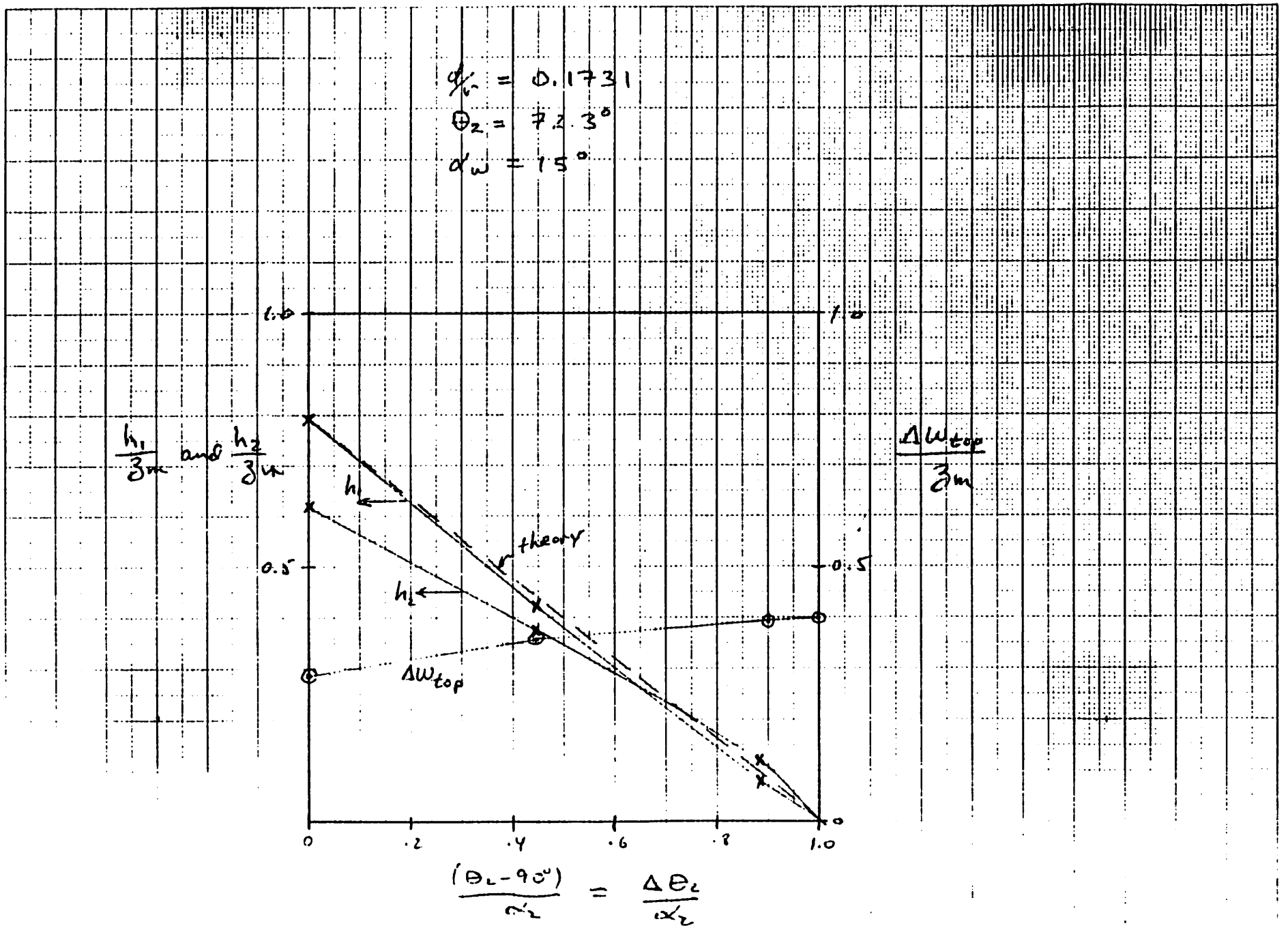

Figure 6 - The effect of resist curvature on metal foot formation

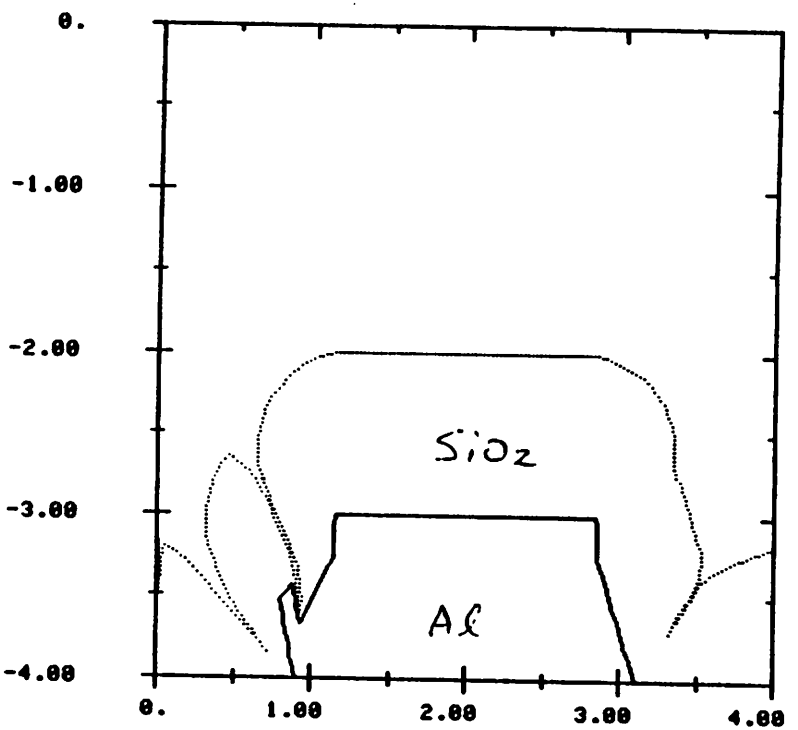

Figure 7 - SAMPLE simulation off sputtered oxide passivation of an aluminum line (post-lift-off) with a large metal foot.

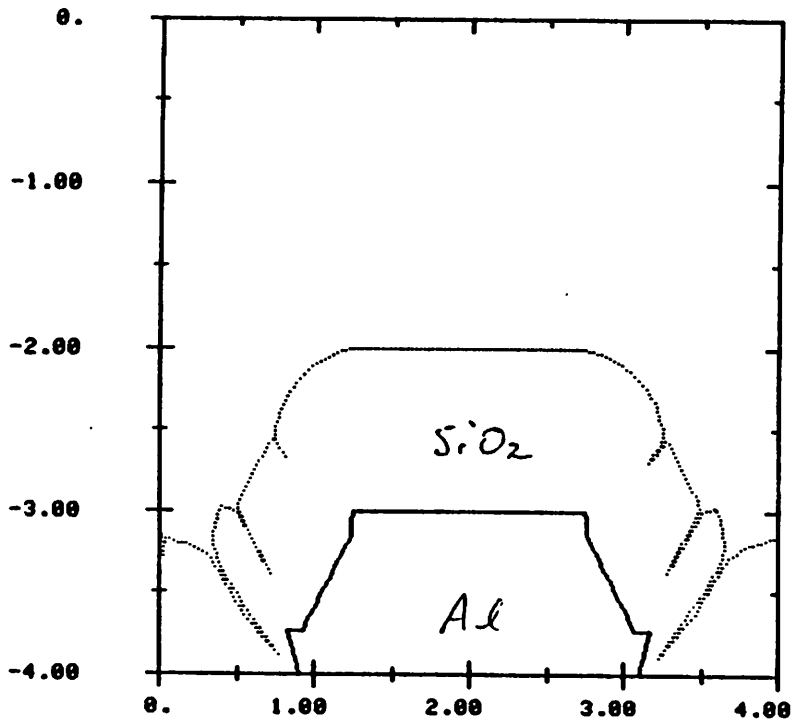

Figure 8 - SAMPLE simulation of sputtered oxide passivation of an aluminum line with small metal feet.

#12 Condition B Resist Profile

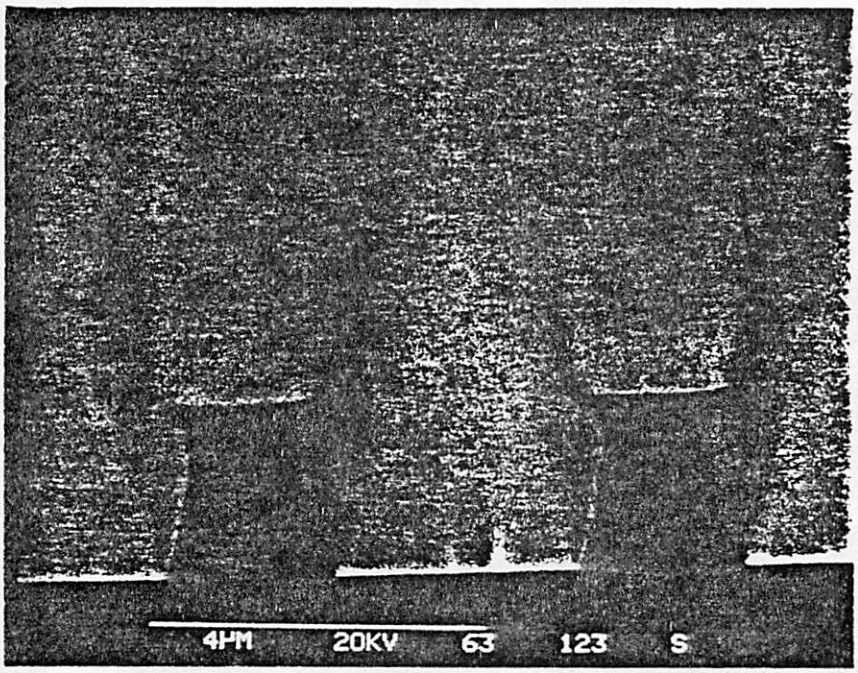

Figure 9

#14 Condition B Blanket Metal

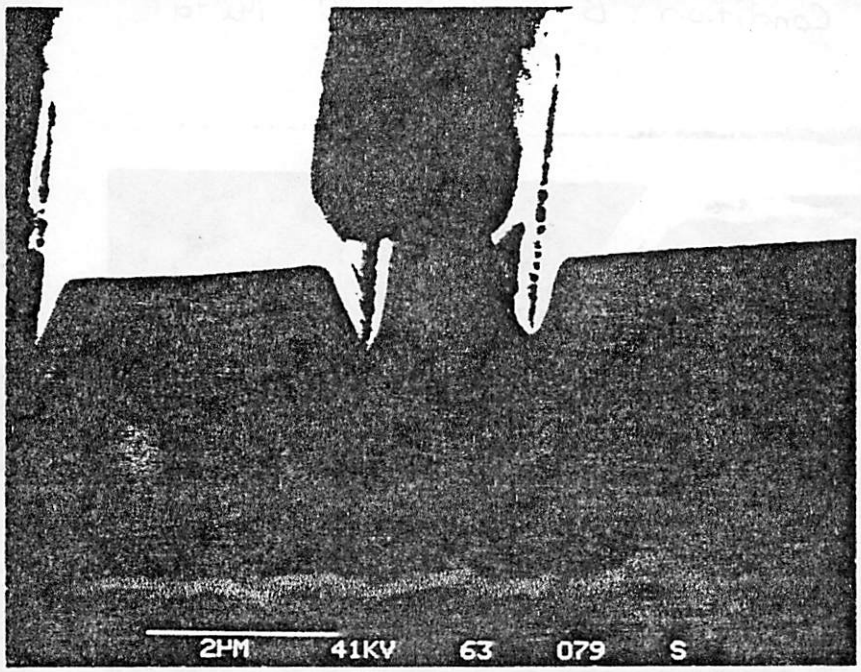

10/31/83 R.J.S.

Figure 10(a)

#16 Condition B Post L/O Metal

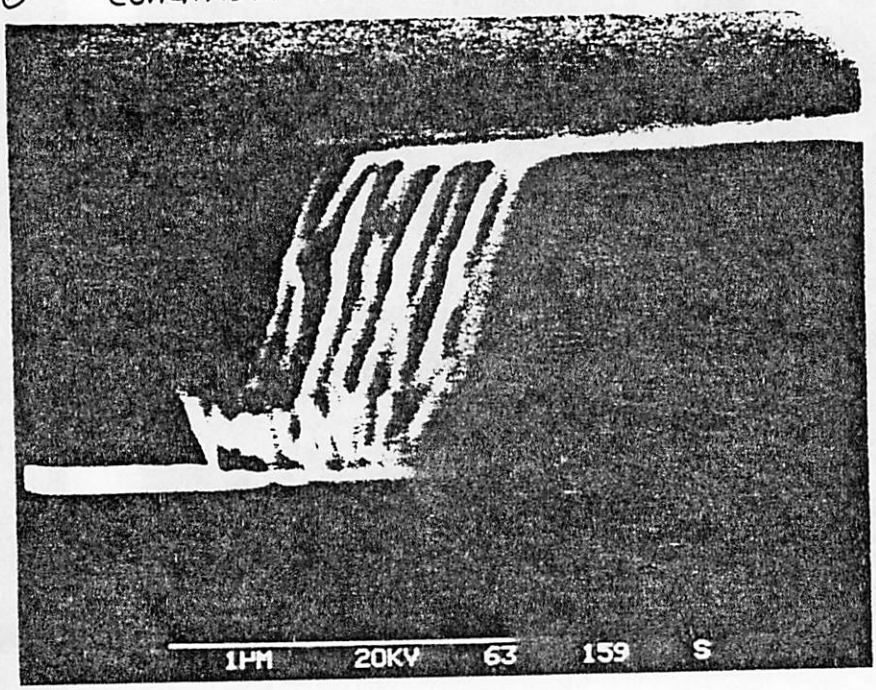

NOTE: LEFT SIDE # 15

Figure 10(b)

#17 Condition B Post L/O Metal

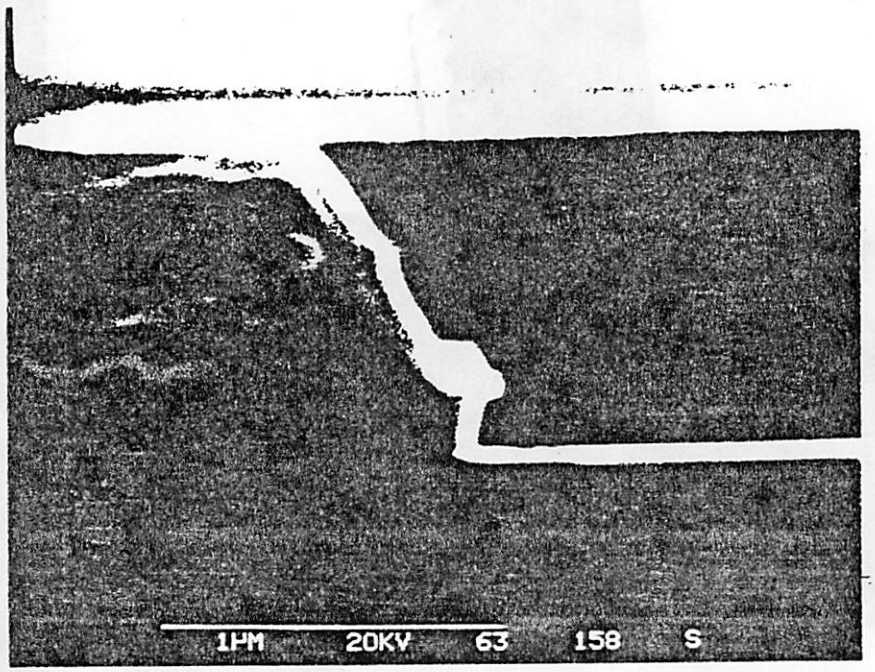

NOTE RIGHT SIDE # 15

Figure 10(c)

#6 CONDITION A Blanked Metal Profile

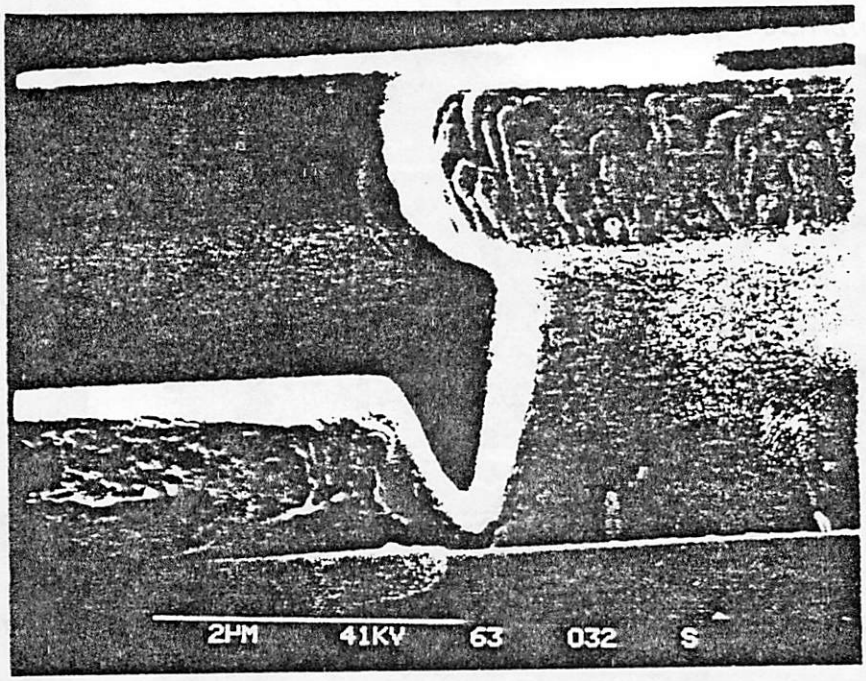

Sample 5 EWC H33 20 KV

(a)

#9 CONDITION A Post L/C Metal

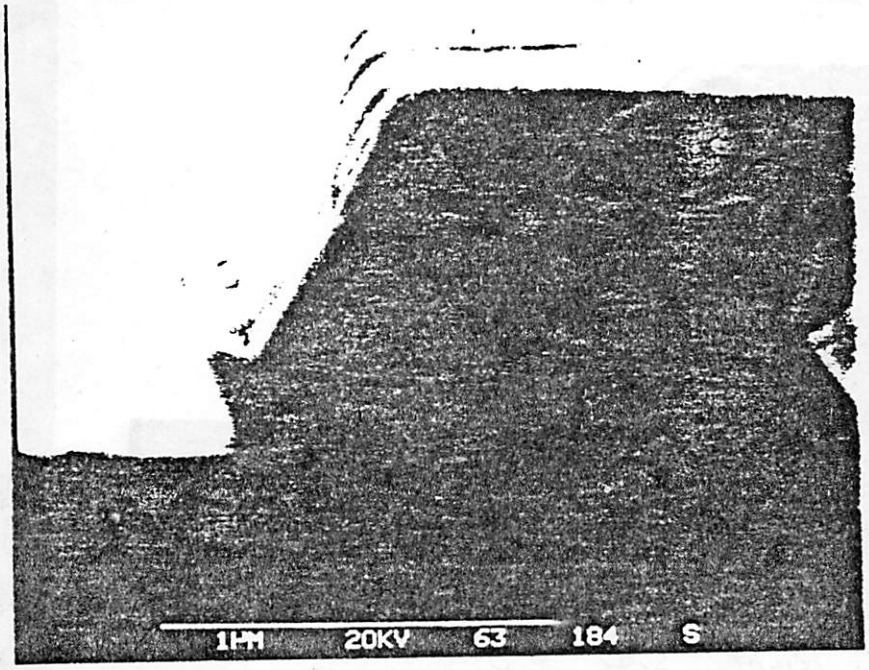

NOTE LEFT SIDE OF #8

(b)

Figure 11

#3 CONDITION A . Blanket Metal Profile

(c)

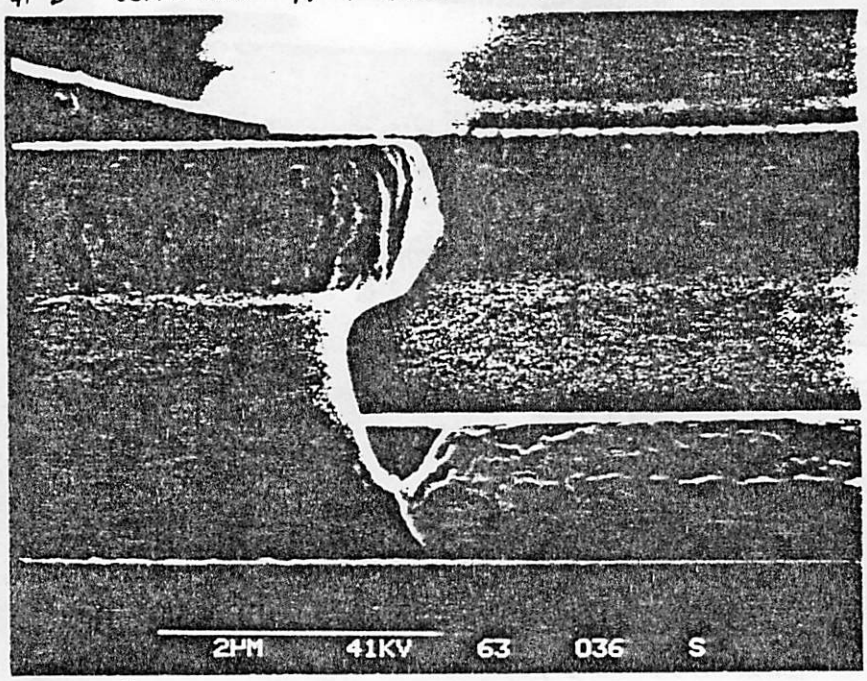

Sample 5 EWS 433 XXX

#10 CONDITION A Post L/C Metal

(d)

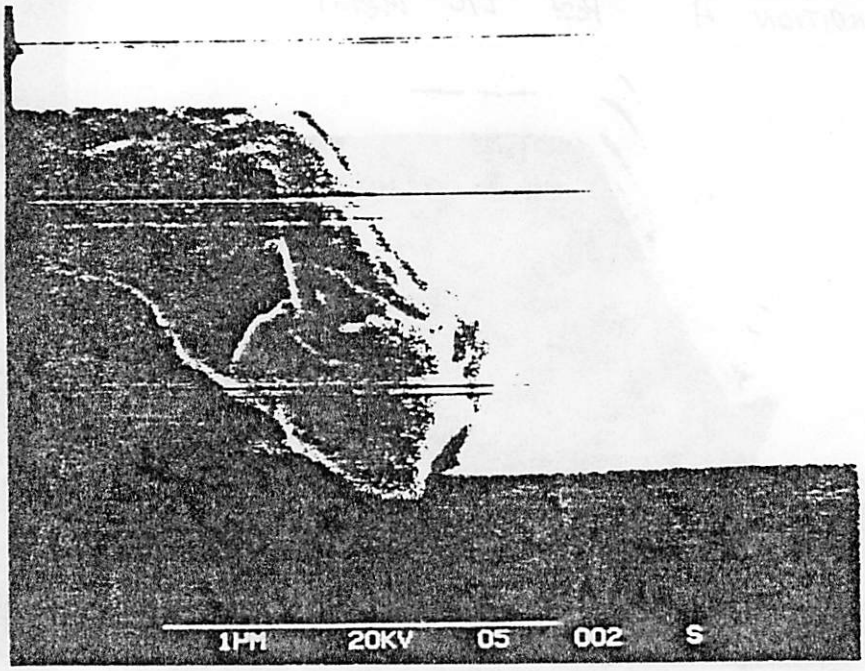

NOTE: Right side #8

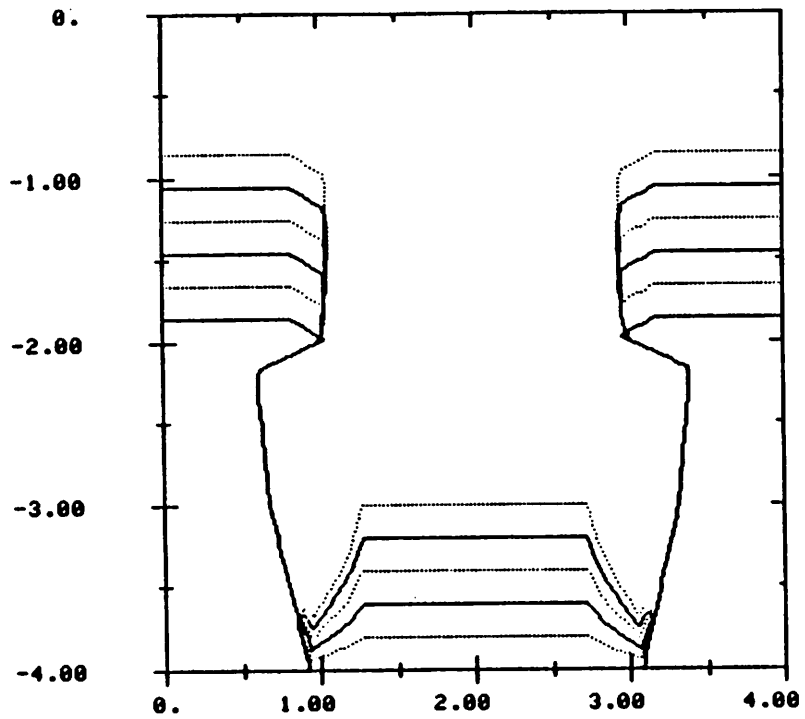

Figure 12 - SAMPLE simulation corresponding to Figure 10.

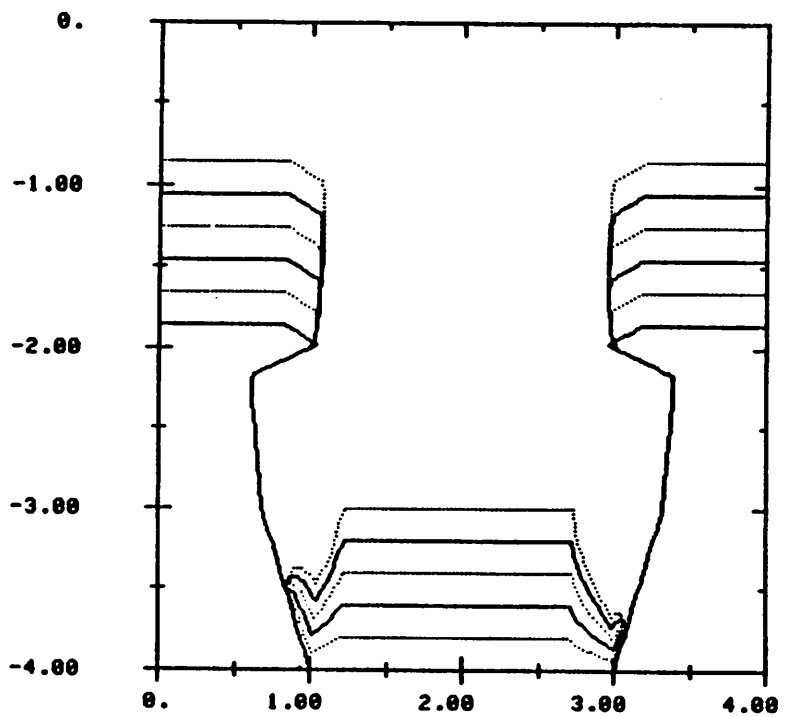

Figure 13. SAMPLE simulation corresponding to Figure 11.

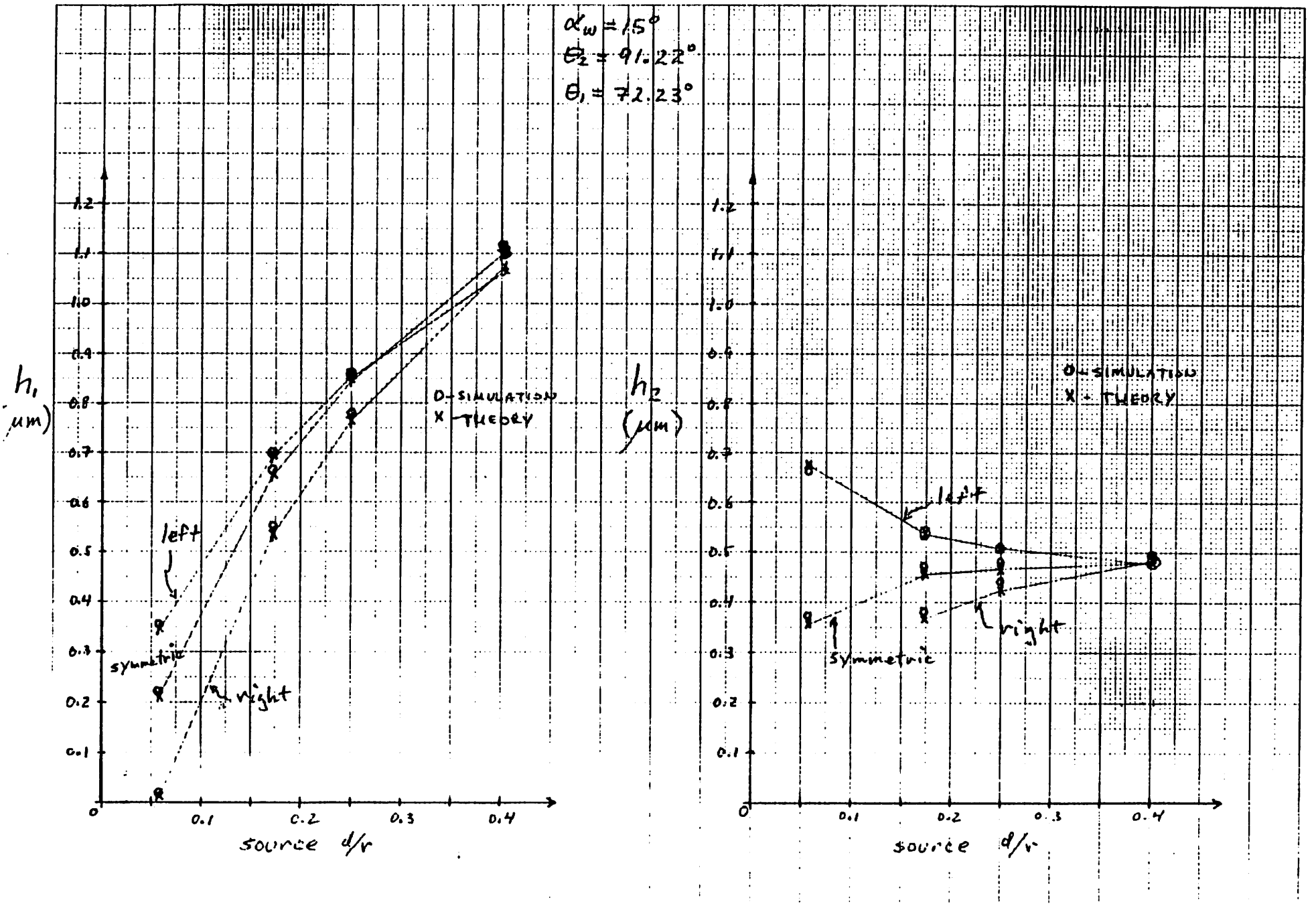
$\alpha_w = 15°$
$\theta_2 = 91.22°$
$\theta_1 = 72.23°$
h_1 (μm)
O-SIMULATION
X-THEORY
left
symmetric
right
source d/r
h_2 (μm)
O-SIMULATION
X-THEORY
left
symmetric
right
source d/r

Figure 14

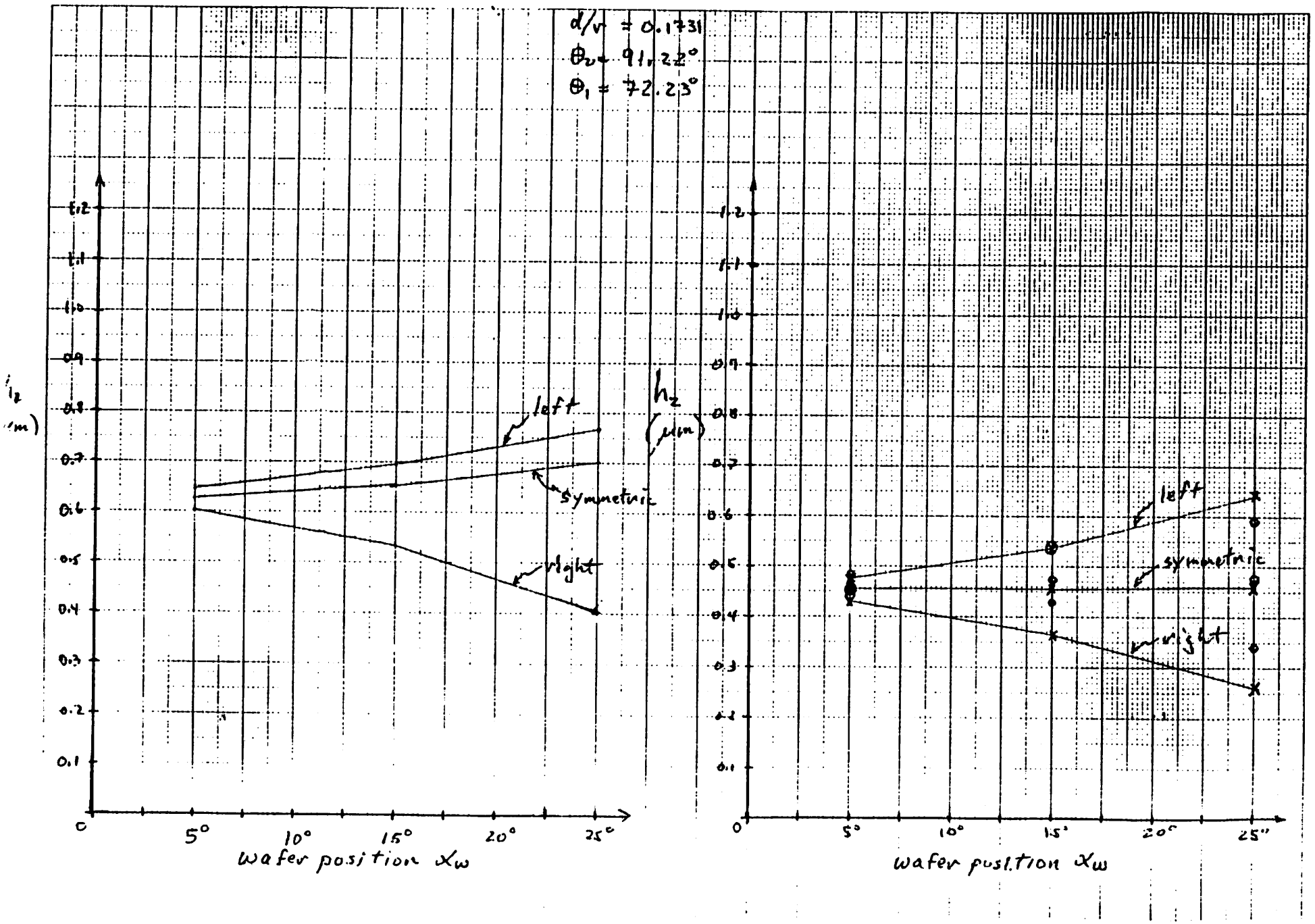
d/r = 0.1731
θ2 = 91.22°
θ1 = 72.23°
h2 (μm)
left
symmetric
right
wafer position xw
0
5°
10°
15°
20°
25°
0.1
0.2
0.3
0.4
0.5
0.6
0.7
0.8
0.9
1.0
1.1
1.2

Figure 15

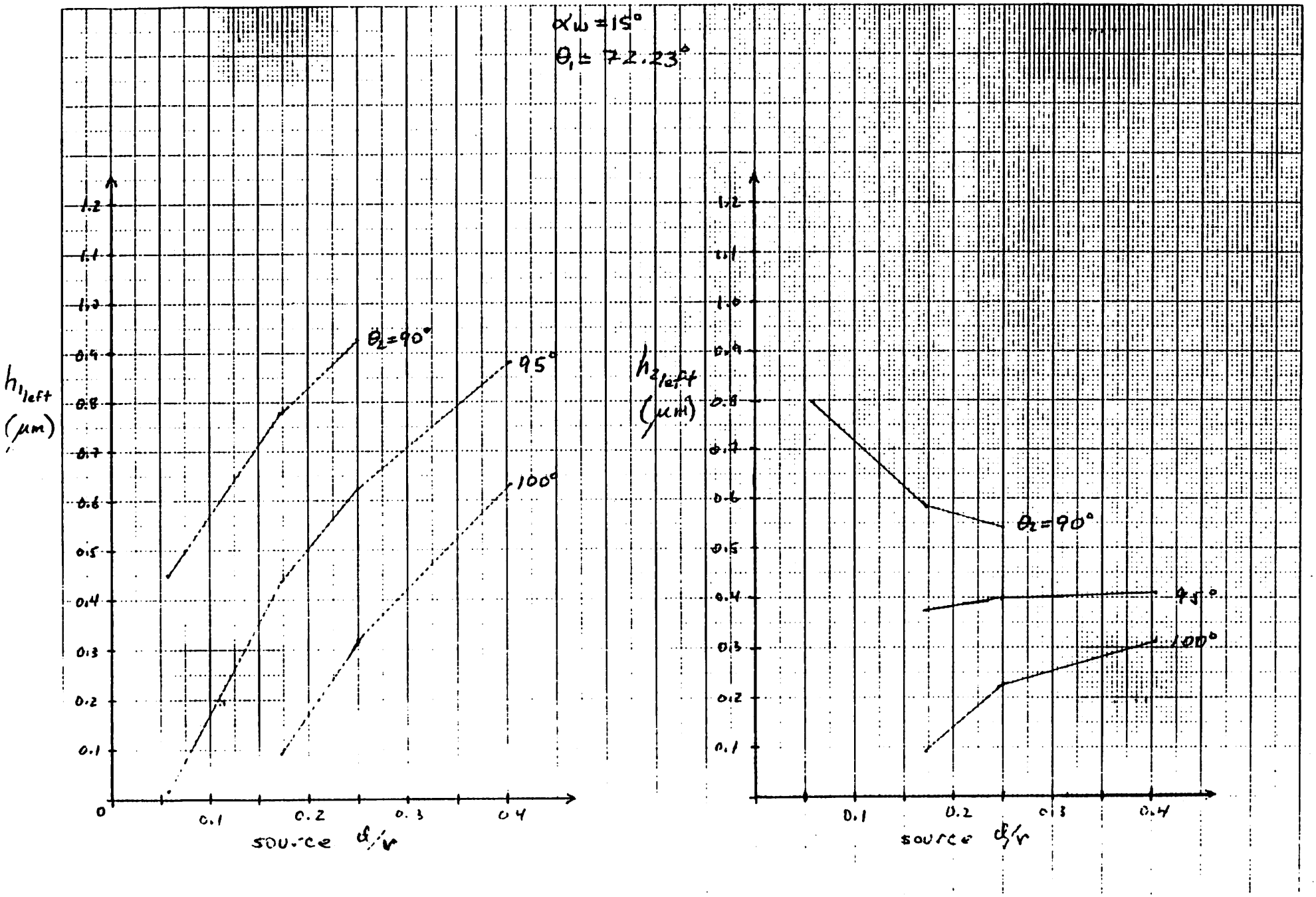
$\alpha_w = 15°$
$\theta_1 = 72.23°$
$h_{1_{left}}$ (μm)
$\theta_2 = 90°$
95°
100°
source d/r
$h_{2_{left}}$ (μH)
$\theta_2 = 90°$
45°
100°
source d/r

Figure 16

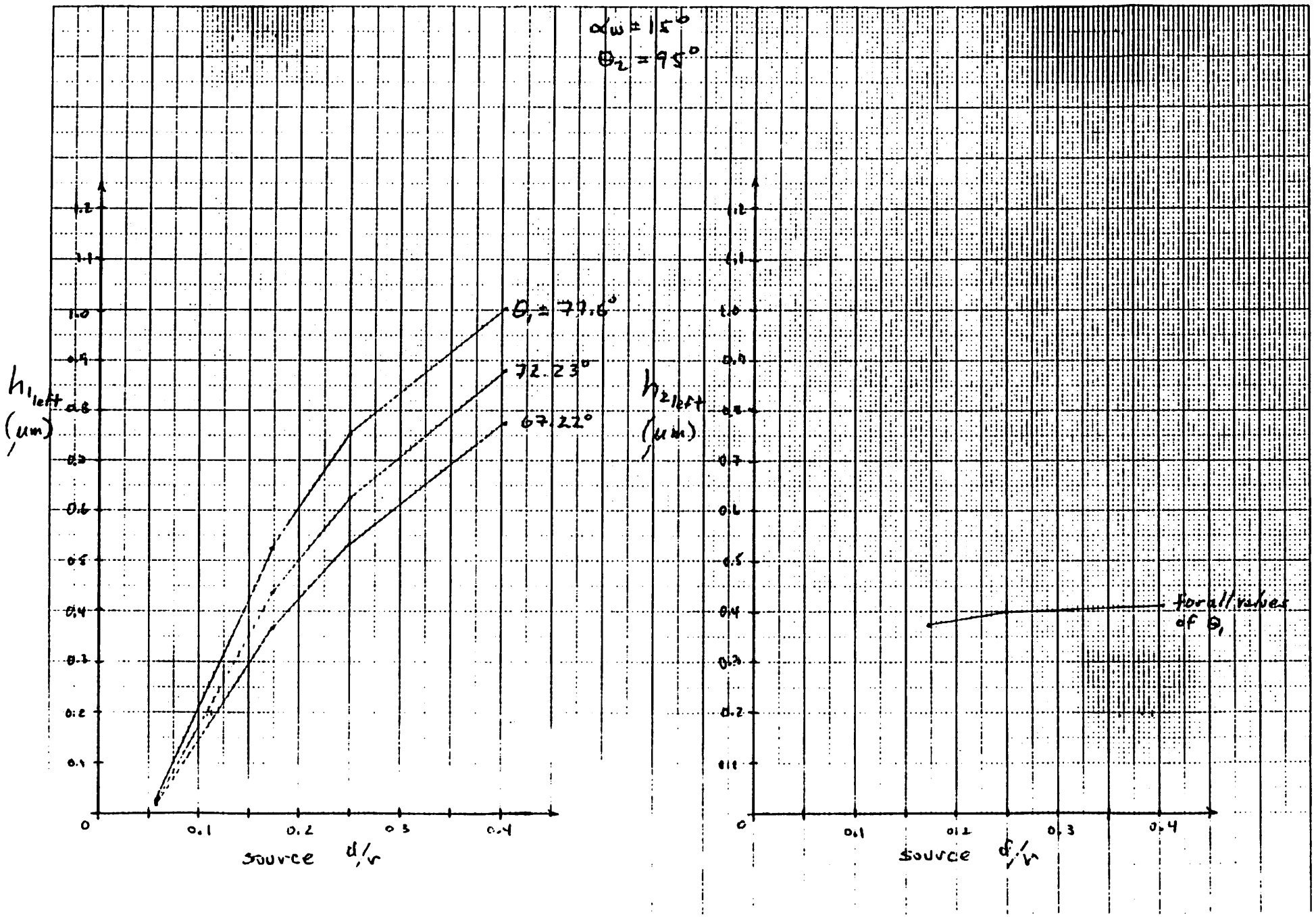

Figure 17

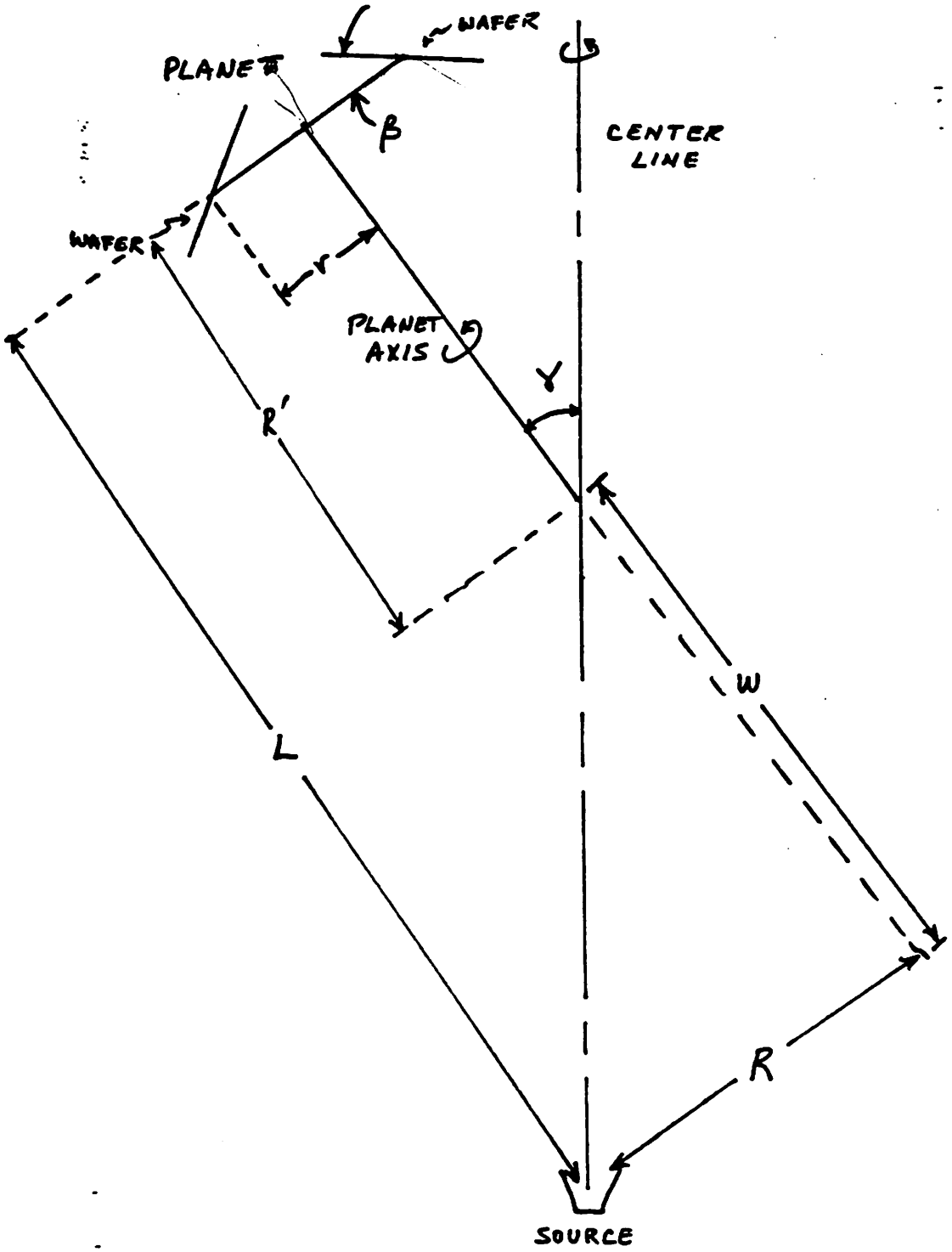

Figure 18 - Configuration of a planetary evaporator.

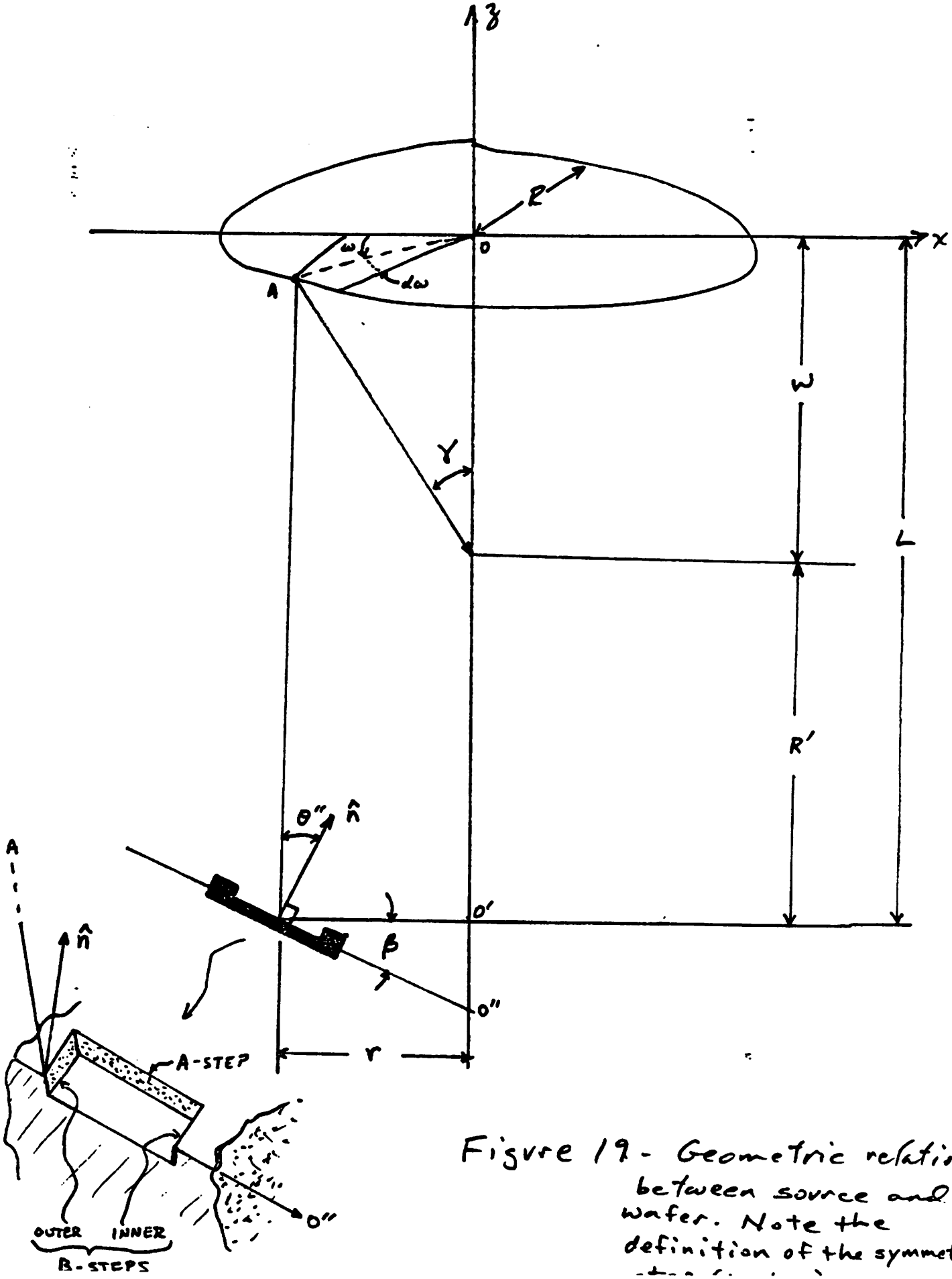

Figure 19 - Geometric relationship between source and the wafer. Note the definition of the symmetric

mrsl

```
trial 50 5 2 4.5 56 0 18 7.5 -0.001 ;
trial 51 1 ;
trial 53 2 1 ;
trial 54 4.0 4.0 ;
trial 55 (0.0,3.4) (2.0,3.4) (2.25,3.3) (2.5,2.95) (2.6,2.75)
(2.6,2.45) (2.65,2.4) (4.0,2.4) ;
trial 58 200, 1500 15 ;
trial 59 ;
%
```

Figure 20 - Input file for simulation a symmetric deposition.

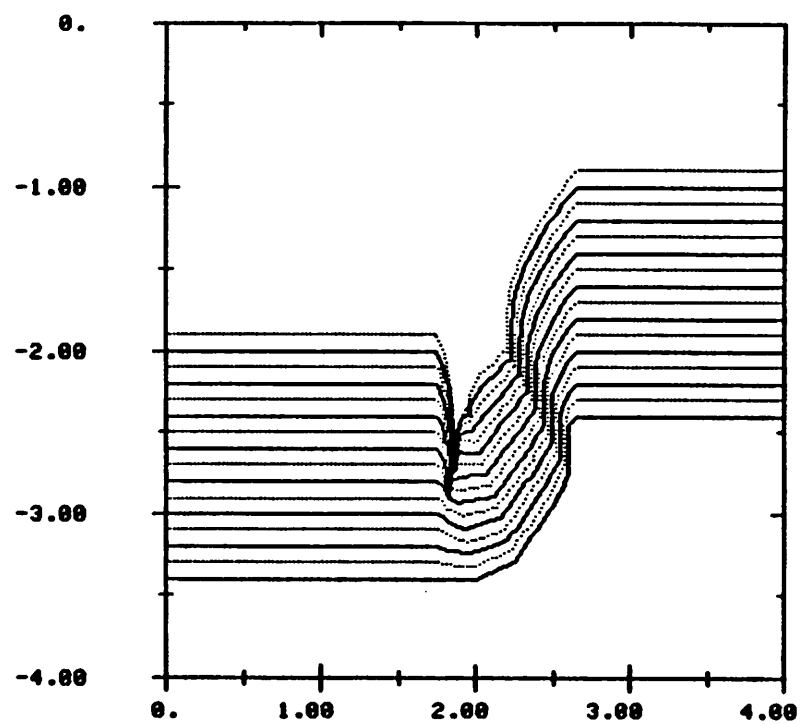

Figure 21 - Resultant profile for the SAMPLE input file given in Figure 20.

```
      sumz=up/bt
      goto 10
20    cosw1 =(1.0-((dl/dr)**2)*((tan(a))**2))**0.5
      cosw2 =-cosw1
      vj1=dr*((1.0+(dl/dr)**2+(rsl/dr)**2-((2.0*rsl/dr)*cosw1))**0.5)
      vj2=dr*((1.0+(dl/dr)**2+(rsl/dr)**2-((2.0*rsl/dr)*cosw2))**0.5)
      diw11=dr**2+dl*dw-(rsl*dr*cosw1)
      diw12=dr**2+dl*dw-(rsl*dr*cosw2)
      diw21=(dr**2+dl**2+rsl**2-(2.0*rsl*dr*cosw1))**1.5
      diw22=(dr**2+dl**2+rsl**2-(2.0*rsl*dr*cosw2))**1.5
      diw3 =(dr**2+dw**2)**0.5
       sumz=0.0
       cstdp1=-dl/vj1
       cstdp2=-dl/vj2
       dwda1=(-(dl/dr)/((cos(a))**2))/cosw1
       dwda2=(-(dl/dr)/((cos(a))**2))/cosw2
       diw1=(diw11/diw21)/diw3
       diw2=(diw12/diw22)/diw3
         sumz1=diw1*dwda1*cstdp1
         sumz2=diw2*dwda2*cstdp2
         sumz = sumz1-sumz2
10    continue
      return
```

```
      sumx=up*tan(a)/bt
      goto 10
20    cosw1 =(1.0-((dl/dr)**2)*((tan(a))**2))**0.5
      cosw2 =-cosw1
      vj1=dr*((1.0+(dl/dr)**2+(rsl/dr)**2-((2.0*rsl/dr)*cosw1))**0.5)
      vj2=dr*((1.0+(dl/dr)**2+(rsl/dr)**2-((2.0*rsl/dr)*cosw2))**0.5)
      diw11=dr**2+dl*dw-(rsl*dr*cosw1)
      diw12=dr**2+dl*dw-(rsl*dr*cosw2)
      diw21=(dr**2+dl**2+rsl**2-(2.0*rsl*dr*cosw1))**1.5
      diw22=(dr**2+dl**2+rsl**2-(2.0*rsl*dr*cosw2))**1.5
      diw3 =(dr**2+dw**2)**0.5
        sumx=0.0
        cstdp1=-dl/vj1
        cstdp2=-dl/vj2
        dwda1=(-(dl/dr)/((cos(a))**2))/cosw1
        dwda2=(-(dl/dr)/((cos(a))**2))/cosw2
        diw1=(diw11/diw21)/diw3
        diw2=(diw12/diw22)/diw3
          sumx1=diw1*dwda1*cstdp1*tan(a)
          sumx2=diw2*dwda2*cstdp2*tan(a)
          sumx = sumx1-sumx2
10    continue
      return
```